Journal of Materials Chemistry

Electronic Supporting Information

CO_2 reverse selective mixed matrix membranes for H_2 purification by incorporation of carbon-silica fillers

Filip de Clippel, Asim L. Khan, Angels Cano-Odena, Michiel Dusselier, Katrien Vanherck, Li Peng, Steffen Oswald, Lars Giebeler, Steven Corthals, Bart Kenens, Joeri F. M. Denayer, Pierre A. Jacobs, Ivo F. J. Vankelecom and Bert F. Sels[*]

Centre for Surface Science and Catalysis
Katholieke Universiteit Leuven
Kasteelpark Arenberg 23, 3001 Heverlee, Belgium
Fax: 32 16 321998, Tel: 32 16 321610
E-mail:bert.sels@biw.kuleuven.be

INDUSTRIAL RELEVANCE OF CO_2:H_2 SEPARATIONS

Synthesis of (bio)hydrogen

By using new processing technologies, hydrogen - a clean energy source - can be produced from CO_2 emitting fossil fuels. Steam or dry reforming of natural gas and controlled gasification of abundant coal combined with carbon capture and storage (*e.g.* CO_2 sequestration) optimises the energy efficiency of the fossil reserves while reducing the environmental impact (Fig. S1).

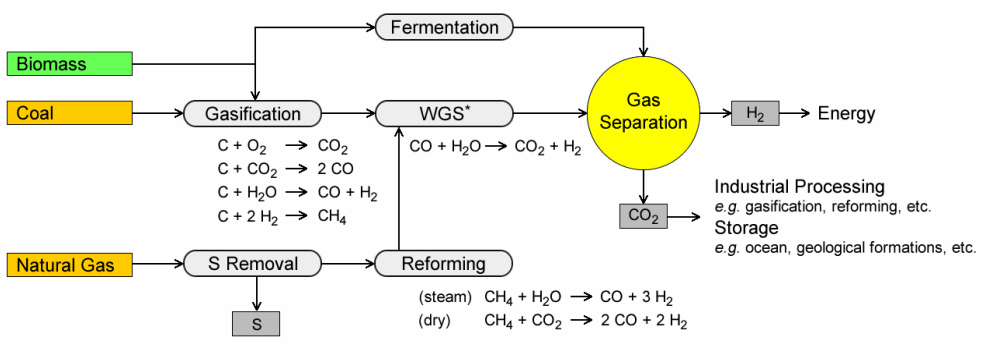

Fig. S1. Various production routes towards H_2 as an energy source and its relation to a growing need of separating CO_2:H_2 gas mixtures (yellow); * Water gas shift reaction. Fossil (orange) and biomass (green) sources.

The former technologies could greatly reduce CO_2 emissions on a short term, but future hydrogen gas will more likely be produced from renewable energy sources (*e.g.* biomass gasification) or by the electrolysis of water. Alternatively, biohydrogen can be produced by bacteria or algae by fermentation and photosynthesis (Fig. S1) as presented in Table S1.

Table S1. Overview of biohydrogen production.

	Reaction	*Organisms*
Dark Fermentation	$C_6O_6H_{12} + 2\ H_2O \rightarrow 2\ CH_3COOH + 2\ CO_2 + 4\ H_2$	(Thermophilic/Facultative) Anaerobic Bacteria
Photo Fermentation	$CH_3COOH + 2\ H_2O \rightarrow 2\ CO_2 + 4\ H_2$	Purple Bacteria, Microalgae
Combined Fermentation	$C_6O_6H_{12} + 6\ H_2O \rightarrow 6\ CO_2 + 12\ H_2$	Fermentative Bacteria
Photolysis	$2\ H_2O \rightarrow O_2 + 2\ H_2$	Microalgae
Indirect Photolysis*	$12\ H_2O \rightarrow 6\ O_2 + 12\ H_2$*	Microalgae, Cyanobacteria
Water Gas Shift	$CO + H_2O \rightarrow CO_2 + H_2$	Fermentative and Photosynthetic Bacteria

* Overall stoechiometric equation after 3 consecutive reactions: i) $6\ H_2O + 6\ CO_2 \rightarrow C_6O_6H_{12} + 6\ O_2$; ii) $C_6O_6H_{12} + 2\ H_2O \rightarrow 2\ CH_3COOH + 2\ CO_2 + 4\ H_2$; iii) $2\ CH_3COOH + 4\ H_2O \rightarrow 4\ CO_2 + 8\ H_2$

State-of-the-Art CO_2 Reverse-Selective Membranes

The transport of gas molecules through a polymeric dense membrane is governed by Fick's laws, hence the selectivity of gas A (over gas B) is expressed by the equation: $\alpha_{A/B} = P_A/P_B = (D_A/D_B) \times (S_A/S_B)$ for which P is the permeability, D the diffusivity and S the apparent solubility constant of the respective gas molecules. Separation with glassy polymeric membranes (*e.g.* polysulphone) is controlled by diffusion, thus favouring migration of the smallest molecule (*e.g.* H_2 in CO_2:H_2 separations). However, the selectivity equation implies that transport of gases in reverse selective membranes is dominated by solubility rather than diffusivity. Therefore, solubility selective membranes *viz.* rubbery polar membranes (*e.g.* PEO) are the preferred choice to separate CO_2 from smaller gas molecules. The solubility, and thus selectivity, can further be enhanced by the addition of polar (*e.g.* carbonyl) or basic (*e.g.* amine) groups inducing an improved interaction of the membrane with the CO_2 molecules.[1,2] An overview of dense and reverse selective membranes, as reported in literature, is presented in Table S2.

Table S2. Overview of the performance of various reverse selective membranes in the separation of CO_2:H_2 gas mixtures.

	P_{CO2} *	$\alpha_{CO2:H2}$ **	*T (K)*	*P (bar)*	T_g *(K)* ***	*Reference*
Pebax®/PEG50	151	10.8	303	0.6	197	Car *et al.*3
55PEO-PA12[a]	120	9.8	308	10.1	218	Bondar *et al.*1[c]
PEGDA 700	95	9.5	296	6.9	*n.d.*	Patel *et al.*4
OIHM75/25[c]	208	9.3	303	3.5	217	Shao and Chung5
PPZ	71	8.5	295	3.6	*n.d.*	Jha and Way6
PEO	12	6.7	308	4.5	221	Lin and Freeman7
PDMS	3070	4.3	308	∞	153	Bondar *et al.*1[c]
CA	6	2.4	303	-	353	Basu *et al.*8
PB/Acrylonitrile (80:20)	63	2.5	308	10.1	*n.d.*	Bondar *et al.*1[c]
XLPEO[b]	390	9.7	308	10.1	209	Lin *et al.*9
PTMEGDA	329	5.6	310	1.0	*n.d.*	Barillas *et al.*[10]
PEGDA	52	4.7	310	1.0	*n.d.*	Barillas *et al.*[10]
PDMS	2848	3.5	310	1.0	153	Barillas *et al.*[10]
PPGDA	102	2.8	310	1.0	n.d.	Barillas *et al.*[10]

[above dashed line] pure gas measurements [below dashed line] mixed (50:50) gas measurements.

* permeability as expressed in Barrer.

** selectivity as determined by P_A/P_B.

*** glass transition temperature (in Kelvin).

[a] 55PEO-PA12 = segmented block copolymer comprised of PEO (55 wt% PE) and PA (nylon-12)

[b] copolymerisation of PEGMEA (99%) and PEGDA (1%) cross linked with PEO

[c] cross-linked organic (PEO) inorganic hybrid membrane (silica content is 25 wt %)

CHARACTERISATION OF FILLERS

N_2 Adsorption: Pore Size Distribution

To take into account the effect of the pore size on the overall membrane performance, N_2 adsorption isotherms were measured on selected composite fillers. Consequently the DFT model was applied on the adsorption branch to determine their pore size distribution. The composite filler with a relatively low carbon loading, *viz.* CSM-1073-18.2, presents a biporous material comprising both mesopores (~21 Å) and micropores (~11 Å and <5Å) (Fig. S2, blue). Upon the increase of the carbon deposition, the mesopores are replaced by micropores as illustrated by the CSM-1073-23.1 filler which contains mostly micropores (<5A and 9 Å) (Fig. S2, red).

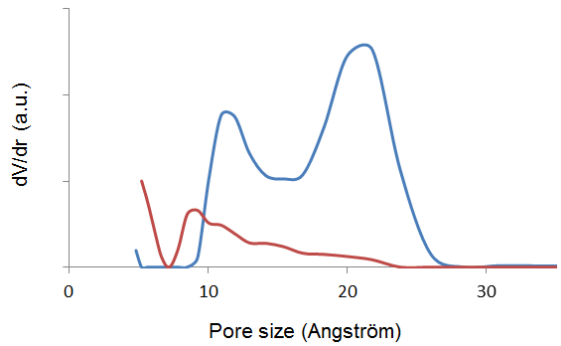

Fig. S2. Pore size distribution of selected CSM fillers as determined according to the DFT method: (red) CSM-1073-23.1, (blue) CSM-1073-18.2.

XPS Analysis

Deconvolution of the C 1s XP spectra of CSMs treated at various temperatures demonstrates an increase of the relative content of graphitic carbon species at higher carbonisation temperature, *viz.* 1073 *vs.* 873 K, as more oxygen is expelled from the carbon network. A low pyrolysis temperature results in a drastic increase of the amount of oxygen surface groups as confirmed by TPD experiments (main text: Table 1). XPS analysis

demonstrates the higher oxygen content is mainly attributed to the presence of carbonyl species to which the peak at 287.3 eV is assigned (Fig. S3).

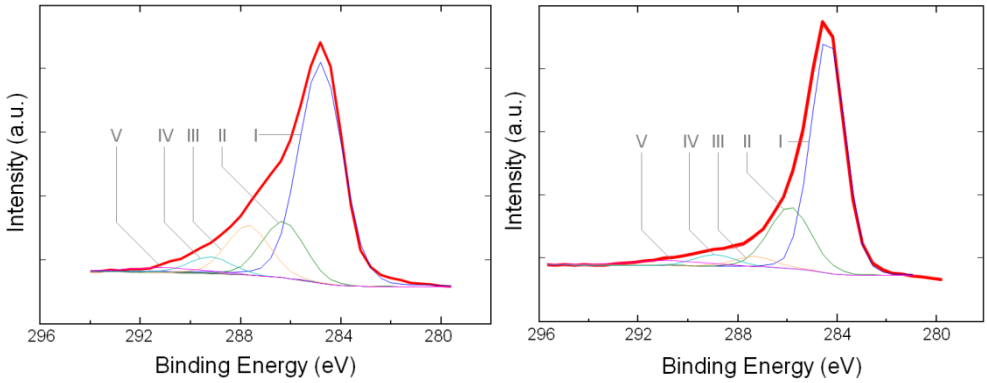

Fig. S3. C 1s XP spectra of a CSM filler pyrolysed at [left] low (CSM-873-23.4) and [right] high pyrolysis temperature (CSM-1073-23.1) and assignment of peak as obtained after deconvolution to various carbon species: I) graphitic, II) phenol/ether/alcohol, III) carbonyl, IV) carboxyl/ester and V) shake-up satellite peaks.

Treatment of CSM-1073-23.1 with nitrogen plasma or ammonium gas resulted in the incorporation of nitrogen species into the carbon network as demonstrated by catalytic burning (main text: Table 1). Deconvolution of the N 1s XP spectra of CSMs allows the assignment of these various nitrogen species. The plasma treated sample (Fig. S4: left), *i.e.* CSM-1073-22.4 / N_2 plasma, shows the dominant presence of pyrrole (400.4 eV), and quaternary (402.3 eV) nitrogen species, next to pyridine (398.7 eV) and nitrogen oxide groups (404.0 eV).

Reaction of ammonia gas with the surface oxygen groups of CSM-1073-23.1 (i.e. CSM-1073-22.4 / NH_3 473 K) results in the formation of (protonated) amide (399.9 / 403.1 eV), imide (399.7 eV) and amine (399.7 eV) functional groups (Fig. S4: right). As no high temperature treatment was applied after contacting the sample with ammonia gas the presence of nitrile, pyridine, pyrrole and quaternary nitrogen species is not expected.

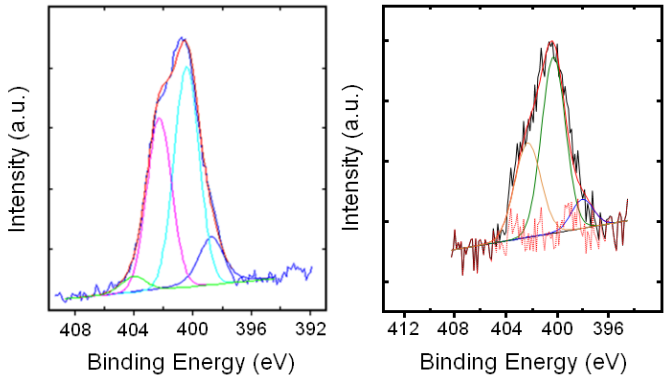

Fig. S4. XPS spectra of nitrogen functionalised fillers: (left) CSM-1073-22.4 / N_2 plasma (right) CSM-1073-18.1 / NH_3 473 K.

Raman Measurements

CSM-1073-23.1 was analysed by Raman spectroscopy (excitation source of 633 nm) before and after nitrogen incorporation by nitrogen plasma or ammonia gas treatment to evaluate the influence of the post-synthesis treatment on the graphitic structure of the CSMs. The intensity ratio I_D/I_G, indicative of the extent of defects in graphitic carbons, of the non-modified sample was determined at 0.97 (Fig. S5: graph a). After nitrogen plasma and ammonia gas treatment, the ratio increased up to 0.98 and 1.05 respectively (Fig. S5: graph b & c), showing a modest deterioration of the sp^2 character of the carbon component. However, the most striking observation is

the strong increase of the luminescence of both the post-treated samples (not show in Fig. S5). This behaviour has been reported before for nitrogen functionalised CNTs and further indicates the successful introduction of nitrogen in the carbon component.[11]

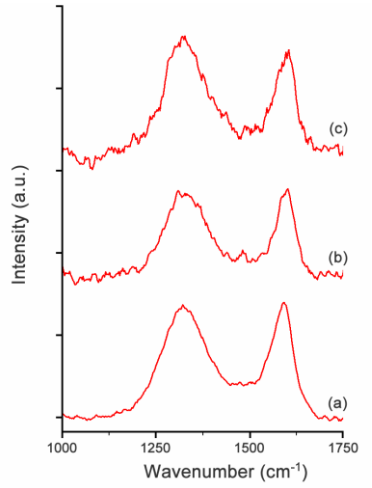

Fig. S5. Baseline corrected and smoothed Raman spectra of CSM-1073-23.1 (a) before and after post synthesis treatment: (b) plasma and (c) ammonia gas mediated functionalisation.

CO_2 Isotherms

CO_2 isotherms of the various filler materials allow for an investigation of their affinity towards CO_2 gas molecules irrespective of the membrane properties. As such, the template silica *viz.* Al-MCM-41 shows a relatively low uptake of CO_2 at low pressures (*e.g.* 0.64 mmol g^{-1} at 0.8 bar) due to the large discrepancy between the pore size of the silica *i.e.* 2.5 nm, and the kinetic diameter of the CO_2 gas molecule *i.e.* 0.33 nm.[12] The introduction of carbon inside the silica pore voids establishes surface oxygen groups that can readily interact with the CO_2 gas molecules. Additionally, smaller pore voids are created that optimise the contact between pore wall and the penetrating gas. Both contributions result in a significant increase of the CO_2 uptake at low pressure, *i.e.* 0.78 mmol g^{-1} at 0.8 bar, as demonstrated for CSM-1073-23.1 (Fig. S6: crosses). The introduction of nitrogen functionalities (e.g. contacting with NH_3 gas at 473 K) further enhances the affinity towards the acidic gas molecules as is demonstrated by the further augmentation, *i.e.* 1.05 mmol g^{-1} at 0.8 bar, of the CO_2 uptake (Fig. S6: squares). Solubility values of the fillers could be calculated by fitting the linear region of the isotherm at low pressure (Fig. S6, right). As such solubility values of 34, 73 and 132 cm^3 cm^{-3} atm^{-1} were obtained for Al-MCM-41, CSM-1073-23.1 and CSM-1073-22.8 / NH_3 473 K respectively.

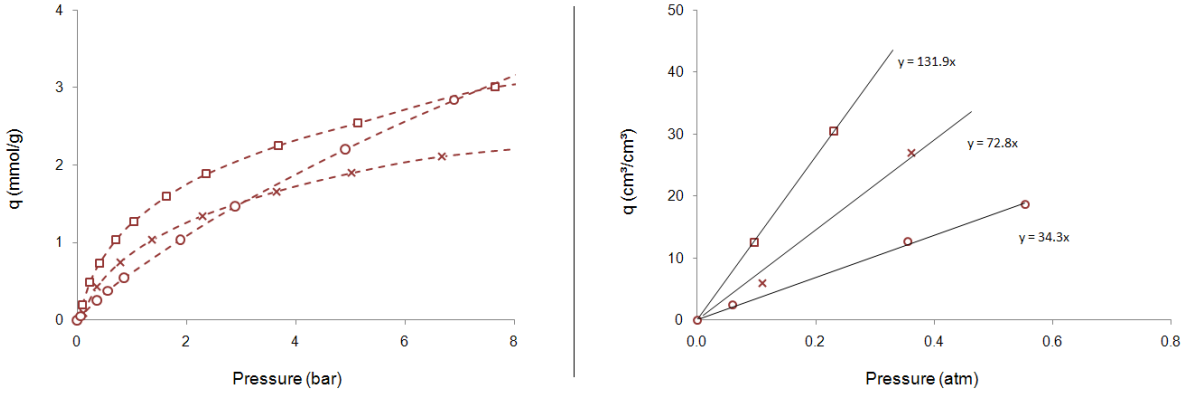

Fig. S6. (left) CO_2 isotherms and (right) detail of the isotherm at low pressure of (o) Al-MCM-41, (x) CSM-1073-23.1 and (□) CSM-1073-22.8 / NH_3 473 K.

MEMBRANE CHARACTERISATION

Analysis of Membrane Structure

The structure of the final MMMs was examined by macroscopic and microscopic observation. An example, representative for the other membranes prepared with CSM fillers, is given by CSM-873-18.7 / N_2 plasma fillers in Fig. S7. All membranes, prepared using the CSM fillers, coloured homogenously black and no cracks could be observed on the membrane surface nor could they be induced by physical bending.

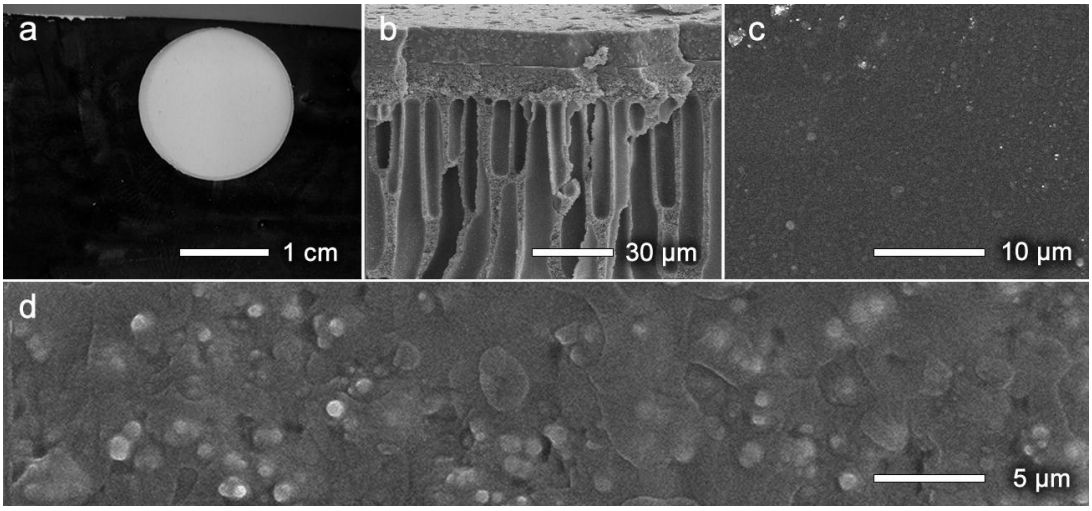

Fig. S7. Typical structure of a MMM prepared with CSM fillers as exemplified by CSM-873-18.7 / N_2 plasma; (a) macroscopic (circular hole was obtained as a membrane piece was cut out for use in the gas separation set-up) and microscopic, *i.e.* SEM, observation: (b) cross-sectional image of the asymmetric multi-layer membrane structure (PP support layer not shown), (c) top surface view demonstrating a crack-free coating, (d) detail of PDMS top layer showing well dispersed CSM particles.

SEM analysis confirmed the absence of cracks on the surface (Fig. S7, c). The average thickness of the different PDMS top-layers was found to be in the range of 10 to 15 µm and only small deviations were observed throughout the full cross section that was examined for each membrane (Fig. S7, b). The homogeneity of the coating was quantified via the standard deviation (main text: Table 1), which was calculated based on the thickness of the membrane on 10 different positions. Detailed SEM pictures of the PDMS top layer show spherical CSM particles immersed in the polymer matrix, confirming the successful dispersion of filler as no voids, *i.e.* defects, between the filler and polymer can be observed (Fig. S7, d).

Swelling tests

The swelling behaviour of the membranes was examined in both polar and non-polar organic solvents. For the non-polar toluene a general decrease of the swelling was observed (Fig. S8). This can be related to the cross-linking of the silanols to the polymer network as well as the good interaction between the fillers and the polymer. In the polar IPA solvent no clear trend could be observed which we suggest is related to the relatively more polar nature of the carbon inside the pore channels which allows for a higher uptake of the IPA molecules. To evaluate the non-polar PDMS polymer, a non-polar solvent *i.e.* toluene gives a better indication of the influence of the fillers on the flexibility of the polymer network.

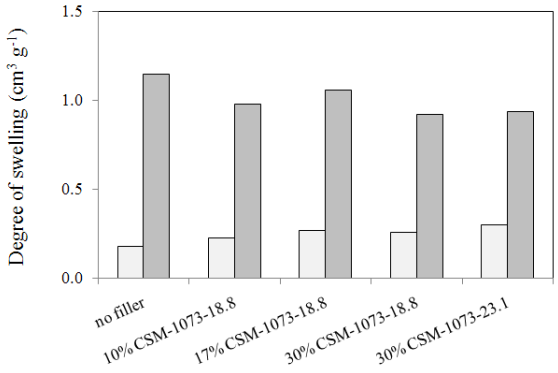

Fig. S8. Swelling behaviour of the PDMS layer as influenced by the addition of fillers in: (light grey) a polar IPA and (dark grey) apolar toluene solvent.

Solvent Resistant Nanofiltration

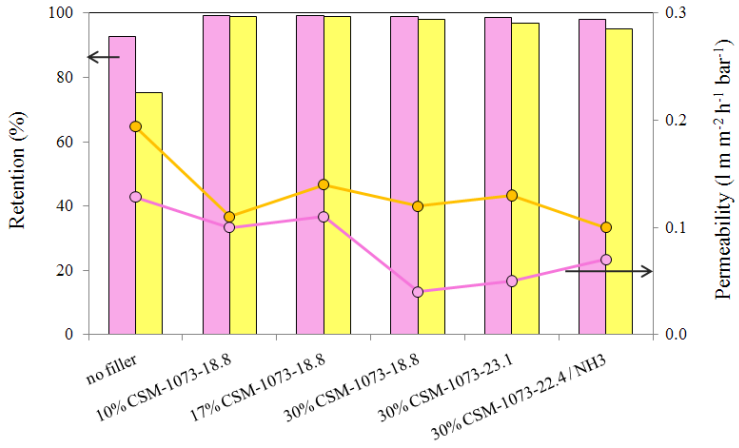

Fig. S9. SRNF of (rose) rose bengal and (yellow) methyl orange using a selection of membranes starting from a 17.5 µM solution in IPA. The retention and permeability are indicated by bars and a line graph respectively.

All membranes were examined in SRNF of methyl orange (327 Da) and rose bengal (1017 Da) in IPA in order to evaluate the presence of defects and the results are shown in Fig. S9. The addition of fillers significantly reduces the permeability of the membranes which is attributed to a densification of the network due to cross linking (see swelling) and an increase of the migration distance of the gas due to the absence of unidirectional pores in the filler material. The increased retention of the dyes is related to the introduction of shape selective properties into the mixed matrix membrane via the microporous CSM (pore size ~ 4.7 A). As such, both observations exclude the presence of defects, and thus macrovoids, between the PDMS polymer and filler material.

Gas separation

Influence of operating conditions

In order for membrane separation to be successfully implemented into various H_2 production processes, all operating at a specific temperature and producing gas mixtures with distinct CO_2 concentrations, the overall effectiveness of the membrane should not be compromised by these variations. To evaluate the influence of these process conditions gas separation was conducted at various temperatures (298 K to 328 K) and CO_2 feed concentrations (10 to 70 vol%). In general an increase of the CO_2 feed concentration or the temperature resulted in the decrease of the CO_2 selectivity as demonstrated in Fig. S10 for various CO_2 concentration at 308 K (Fig. S10, left) and various temperatures at a CO_2 feed concentration of 10 % (Fig. S10, right).

A reduction of the CO_2 selectivity with temperature is independent of the filler's presence, thus can be assigned to the permeation of the gases in the polymer matrix. Selectivity of these rubbery PDMS membranes is dominated by solubility. The critical temperature of both gases, *viz.* 33 and 304 K for H_2 and CO_2 respectively, implies a superior condensability of the latter. By consequence the negative impact of the temperature on the solubility is stronger for CO_2 in comparison to H_2 whose overall permeance is enhanced by the increase of the diffusability of the gas.[13]

An increase of the CO_2 concentration in the feed gas mixture is attended with a drop of the CO_2 selectivity. In general this behaviour is explained by plasticisation of the membrane and originates from a strong interaction of the penetrating gas molecules with the polymer which increases the free volume and chain mobility of the polymer. Substantial swelling has been reported for the CO_2-philic PDMS membranes.[14] However, for reverse selective membranes the increase of the free volume could result in an increase of the selectivity if many shape selective sites are present.[15] However, the liquid like matrix of PDMS does not exert shape selective properties. The reduced selectivity is thus assigned to an increased permeation of H_2.

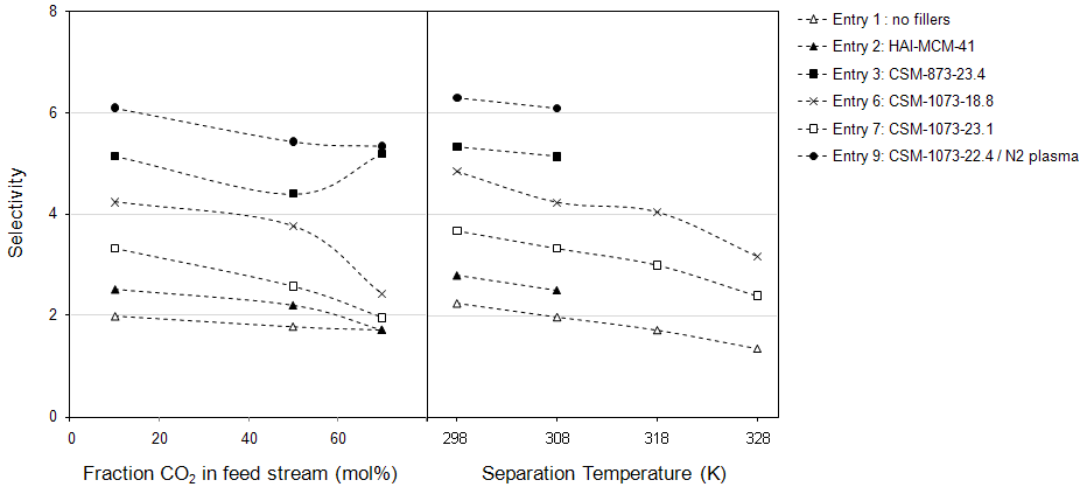

Fig. S10. Influence of [left] CO_2 concentration in the feed gas mixture as (evolution shown at 308 K) and [right] operating temperature (evolution shown for CO_2 feed concentration of 10%). Type of filler in the MMMs are indicated. Entries are assigned according to table 1 in main text.

REFERENCES

1 (a) W.J. Koros, *J. Polym. Sci. Polym. Phys. Ed.*, 1985, **23**, 1611. (b) S.G. Kazarian, M.F. Vincent, F.V. Bright, C.L. Liotta and C.A. Eckert, *J. Am. Chem. Soc.*, 1996, **118**, 1729. (c) V.I. Bondar, B.D. Freeman and I. Pinnau, *J. Polym. Sci. Part B: Polym. Phys.*, 2000, **38**, 2051.
2 K. Ghosal, R.T. Chern, B.D. Freeman, W.H. Daly and I.I. Negulescu, *Macromolecules*, 1996, **29**, 4360.
3 A. Car, C. Stropnik, W. Yave and K.-V. Peinemann, *J. Membrane Sci.*, 2008, **307**, 88.
4 N.P. Patel, A.C. Miller and R.J. Spontak, *Adv. Mater.*, 2003, **15**, 729.
5 L. Shao and T.-S. Chung, *Int. J. Hydrogen Energ.*, 2009, **34**, 6492.
6 P. Jha and J.D. Way, *J. Membrane Sci.*, 2008, **324**, 151.
7 (a) H. Lin and B.D. Freeman, *J. Mol. Struct.*, 2005, **739**, 57. (b) H. Lin and B.D. Freeman, *J. Membrane Sci.*, 2004, **239**, 105.
8 S. Basu, A.L. Khan, A. Cano-Odena, C. Liu and I.F.J. Vankelecom, *Chem. Soc. Rev.*, 2009, **39**, 750.
9 H. Lin, E. Van Wagner, B.D. Freeman, L.G. Toy and R.P. Gupta, *Science*, 2006, **311**, 639.
10 M.K. Barillas, R.M. Enick, M. O'Brien, R. Perry, D.R. Luebke and B.D. Morreale, *J. Membrane Sci.*, 2011, **372**, 29.
11 W. Huang, S. Fernando, L.F. Allard and Y.-P. Sun, *Nano Lett.*, 2003, **3**, 565.
12 T.G. Glover, K.I. Dunne, R.J. Davis and M.D. LeVan, *Micropor. Mesopor. Mater.*, 2008, **111**, 1.
13 T.C. Merkel, R.P. Gupta, B.S. Turk and B.D. Freeman, *J. Membrane Sci.*, 2001, **191**, 85.
14 N.M.B. Flichy, S.G. Kazarian, C.J. Lawrence and B.J. Briscoe, *J. Phys. Chem. B*, 2002, **106**, 754.
15 H. Lin, E. Van Wagner, B.D. Freeman, L.G. Toy, R.P. Gupta, *Science*, 2006, **311**, 639.